Available online at www.sciencedirect.com

ScienceDirect

Advances in Space Research 64 (2019) 143–158

ADVANCES IN SPACE RESEARCH (a COSPAR publication)

www.elsevier.com/locate/asr

Anomalous seismo-LAI variations potentially associated with the 2017 $M_w = 7.3$ Sarpol-e Zahab (Iran) earthquake from Swarm satellites, GPS-TEC and climatological data

Mehdi Akhoondzadeh [a,*], Angelo De Santis [b], Dedalo Marchetti [c,b], Alessandro Piscini [b] Shuanggen Jin [c]

[a] *Remote Sensing Division, School of Surveying and Geospatial Engineering, College of Engineering, University of Tehran, Tehran, Iran*
[b] *Istituto Nazionale di Geofisica e Vulcanologia, Roma, Italy*
[c] *School of Remote Sensing and Geomatics Engineering, Nanjing University of Information Science and Technology, Nanjing 210044, China*

Received 22 November 2018; received in revised form 11 March 2019; accepted 14 March 2019
Available online 23 March 2019

Abstract

The $M_w = 7.3$ earthquake near the Iran-Iraq border in west Iran (34.911°N, 45.959°E) occurred at 18:18:17 UTC (LT = UTC + 03:30), November 12, 2017 as the result of oblique-thrust faulting at mid-crustal depth (~19 km). Median, Kalman filter and Neural Network, as three standard, classical and intelligent methods, have been implemented to investigate three months of GPS Total Electron Content (TEC) measurements and to detect the striking anomalous variations around the time and location of the mentioned earthquake. The first method detects unusual variations, 9 days before the event, between 21:00 and 22:00 UTC. The other two methods of Kalman filter and Neural Network detect another clear anomaly on 11 days preceding the earthquake at 16:00 UTC. These findings are two of the outstanding results of GPS-TEC precursor analysis. This paper also presents the results of Swarm satellites (Alpha, Bravo and Charlie) data analysis inside the Dobrovolsky area around the Iran earthquake epicenter during the period from 1 August to 30 November 2017. The time series and orbital analysis of six measured parameters including electron density, electron temperature, magnetic scalar and vectors (X, Y, Z) components indicate irregular variations between 8 and 11 days prior to the occurrence of the earthquake. Since the variations of the solar and geomagnetic indices follow a normal behaviour during the whole period of the observed ionospheric anomalies between 8 and 11 days before the earthquake, it can be concluded that multi-precursors analysis has an important role to acknowledge the seismo-LAI (Lithospheric-Atmospheric-Ionospheric) anomalies associated to strong earthquakes such as this case. Furthermore, some physical and chemical atmospheric parameters from a climatological database are investigated and some interesting anomalies above two standard deviations prior to the earthquake are found. This paper shows not only anomalies in atmosphere and ionosphere but also a contemporary analysis of different data sources to detect the possible Lithosphere Atmosphere Ionosphere Coupling (LAIC) effects.
© 2019 COSPAR. Published by Elsevier Ltd. All rights reserved.

Keywords: Pre-earthquake anomaly; Ionosphere; Swarm satellites; GPS TEC; LAIC mechanism

1. Introduction

Some previous scientific reports indicate some pre-seismic anomalous variations in lithosphere, atmosphere and ionosphere disturbances that, after excluding man-made, seasonal, solar and geomagnetic disturbances, may

* Corresponding author.
E-mail address: makhonz@ut.ac.ir (M. Akhoondzadeh).

https://doi.org/10.1016/j.asr.2019.03.020
0273-1177/© 2019 COSPAR. Published by Elsevier Ltd. All rights reserved.

be considered potential earthquake precursors (Parrot, 1995; Liu et al., 2004; Hayakawa and Molchanov, 2002; Pulinets and Boyarchuk, 2004; Freund, 2009; Pulinets and Ouzounov, 2011; Sorokin and Pokhotelov, 2014). The ionospheric anomalies can be observed in the D, E and F layers, about 1–10 days before a strong earthquake and continue a few days after the event, while it is still challenging to detect exact pre-earthquake anomalies (Jin et al., 2015). In this work we will analyse a case study concerning, in the border region between Iran and Iraq close to Sarpol-e Zahab town (34.911°N, 45.959°E, 19.00 km depth), a strong earthquake of $M_w = 7.3$ took place at 18:18:17 UTC (LT = UTC + 03:30 = 21:48) on November 12, 2017 (Fig. 1). This earthquake is the largest seismic event after the M7.4, 1909 AD Sialkhor earthquake near the Borujerd city in the Zagros region.

Recently the expanded network of GPS receivers has generated an increasing amount of data regarding the ionosphere state. Total Electron Content (TEC) is the integrated number of the electrons within the line between the satellite and receiver or between two satellites. Since the time series of GPS-TEC follow non-linear variations, in addition to Median method, two other classical and intelligent algorithms including Kalman filter and Neural Network have been implemented to observe the irregular variations. The detailed descriptions of these three methods can be found in Akhoondzadeh (2012 and 2013).

Swarm is currently one of the main satellite missions that provides free available data and can be used to monitor some of the important parameters of the ionosphere continuously. Swarm mission (launched in 2013) is an ESA constellation of three twin satellites, namely Alpha (A), Bravo (B) and Charlie (C), carrying the same payload of multi instruments and sensors. In particular, in this paper we will use the data from: (1) The absolute scalar magnetometer (ASM) that measures the strength of the magnetic field and provides scalar measurements of the magnetic field to calibrate the vector field magnetometer;

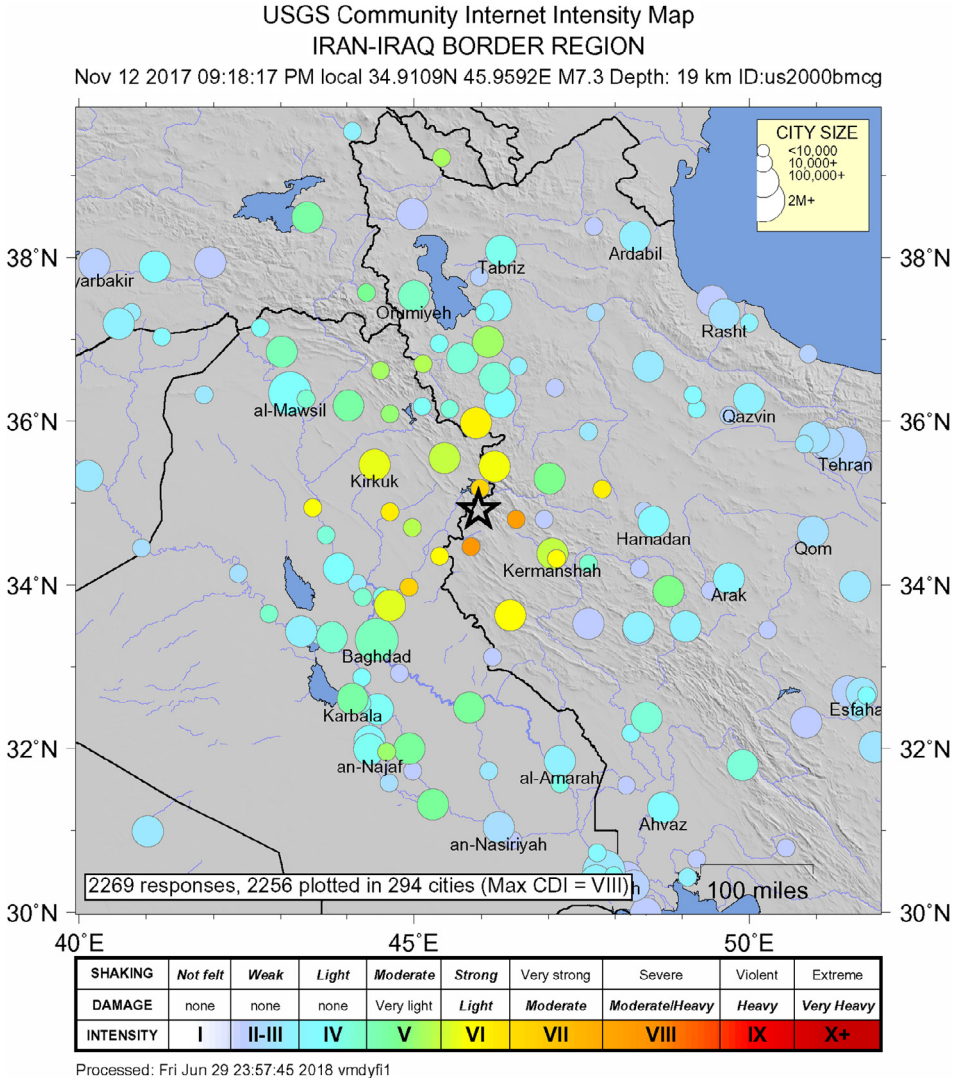

Fig. 1. The geographic location of the 2017 Sarpol-e Zahab earthquake epicenter in the border region between Iran and Iraq. A star represents the epicenter (https://earthquake.usgs.gov/earthquakes).

(2) The vector field magnetometer (VFM) which makes high-precision measurements of the magnitude and direction of the magnetic field; (3) EFI instrument that is composed by Langmuir Probe and Thermal ion Imager. Langmuir Probe provides plasma data electron density Ne, electron temperature Te and spacecraft potential V (Haagmans et al., 2013).

To deeply understand the preparation phase of an earthquake, in this study we introduce also an investigation of the Earth's surface and physical/chemical composition of the atmosphere as we expected some alteration before a great earthquake (Pulinets and Ouzounov, 2011). We investigate the skin temperature SKT and total column water vapour (TCWV) from ERA-Interim and real-time data provided by the European Center for Medium-range Weather Forecast (ECMWF) (Dee et al., 2011) and Total Aerosol Thickness (AOT) and Sulphur Dioxide (SO_2) from Modern-Era Retrospective analysis for Research and Applications, Version 2 (MERRA-2) database provided by NASA (Gelaro et al., 2017).

Although many single case studies have already been done in the field of pre-seismic ionospheric anomalies, we are confident that adding other multi-data anomaly analysis will decrease the corresponding uncertainty and, eventually, help to identify a chain of processes behind the preparation of the earthquake of interest. Therefore, in this study using the GPS- TEC data and the measured parameters from electric field instrument and absolute and vector field magnetometers on board each Swarm satellite, a comparative study has been performed to detect the striking anomalies around the time and location of the 2017 Iran Sarpol-e Zahab earthquake.

To explore possible pre-seismic anomalies in this event, Wu et al. (2018) utilized a multiparameter method to analyze three satellite retrievals, including surface latent heat flux (SLHF), surface skin temperature (SST) and aerosol optical depth (AOD). They observed that, for Ms.7.3 Iran Sarpol-e Zahab earthquake shocked on November 12, 2017, a spot-shaped region with highly anomalous SLHF values occurred in the west of epicenter two weeks before the mainshock. A strip-shaped high-value AOD anomaly was also found at the north Iraq-Iran border 12 days before the mainshock.

In addition, Liu (2018) investigated seismo-ionospheric precursors of the 2017 M7.3 Sarpol-e Zahab earthquake and the 2018 M5.9 Osaka earthquake observed by FORMOSAT-5/AIP.

2. Observations and data analysis

2.1. Solar and geomagnetic indices

The ionospheric parameters are affected by Space Weather (SW) phenomena including solar flares and coronal mass ejection (CMEs) that could produce at Earth's orbit geomagnetic storms especially in the equatorial and polar regions of the planet. The auroral activity has an important role in the mid-latitude ionosphere perturbations, as some time the auroral ring currents could move to little lower latitudes and/or create penetrating electrical field currents in mid latitude regions. In other words, the ionosphere currents and equatorial storm-time ring current in periods of solar-terrestrial disturbances produce significant geomagnetic field disturbances observed down to the ground. Accordingly, the measured ionospheric plasma parameters may display variations during and in absence of seismic activity. Therefore, it is difficult to separate pre-seismic ionospheric phenomena from the ionospheric disturbances due to the solar-terrestrial activities. Consequently, to differ the potential seismo-ionospheric perturbations from solar geomagnetic disturbances, the indices of Kp, a_p, D_{st} and F10.7 were checked. Despite a_p is extracted by Kp, both indices are shown as in this work we used alternatively both of them. The detected irregular variations of ionosphere in quiet solar geomagnetic conditions ($Kp < 2.5$, $Dst > -20$ nT, $Dst < 20$ nT and $F10.7 < 120$ SFU) may be associated with seismic activities. The biggest difference between the ionospheric effects caused by geomagnetic storm and possible seismogenic effects is that the former has a global impact being observed all over the world while, the latter is observed only by stations with distance less than one-two thousands km from the potential epicenter (Pulinets and Boyarchuk, 2004).

Fig. 2 illustrates the variations of K_p, a_p, D_{st} and F10.7 indices, during the period of 01 September to 30 November 2017. An asterisk (in Fig. 2a–c) or a vertical dashed line (Fig. 2d) indicates the earthquake time. The x-axis represents the days relative to the earthquake day. A high geomagnetic activity is clearly observed on 8 September 2017, when the K_p and a_p indices reach the maximum values of 8.3 and 236, respectively, between 13:00 and 15:00 UTC. Another unusual variation of the K_p and a_p indices is also seen on 4 days before the earthquake between 13:00 and 15:00 UTC with the values of 5 and 48. Irregular D_{st} values are observed on 4 days before the event when this parameter exceeds the lower boundary value (i.e. −20 nT), reaching the value of −65 nT at 17:00 UTC. D_{st} value has a minimum value of −124 nT during the studied time period on 8 September 2017 at 02:00 UTC. The F10.7 value gradually increases from about 01 September and reaches the maximum value of 182.50 SFU on 04 September 2017 (69 days before the event), then gradually decrease till reaching, after around ten days, with some light fluctuations an almost constant value around 70–80 SFU.

2.2. GPS-TEC data analysis

Fig. 3(a) shows TEC variations derived from GIM data and the closest node (35°N, 45°E) to the epicenter during the period of 1 September to 30 November 2017. By visual inspection and without performing any special analysis, unusual TEC values are clearly seen on around 8 September. However, as mentioned before, the geomagnetic indices show high activities on this time and therefore the

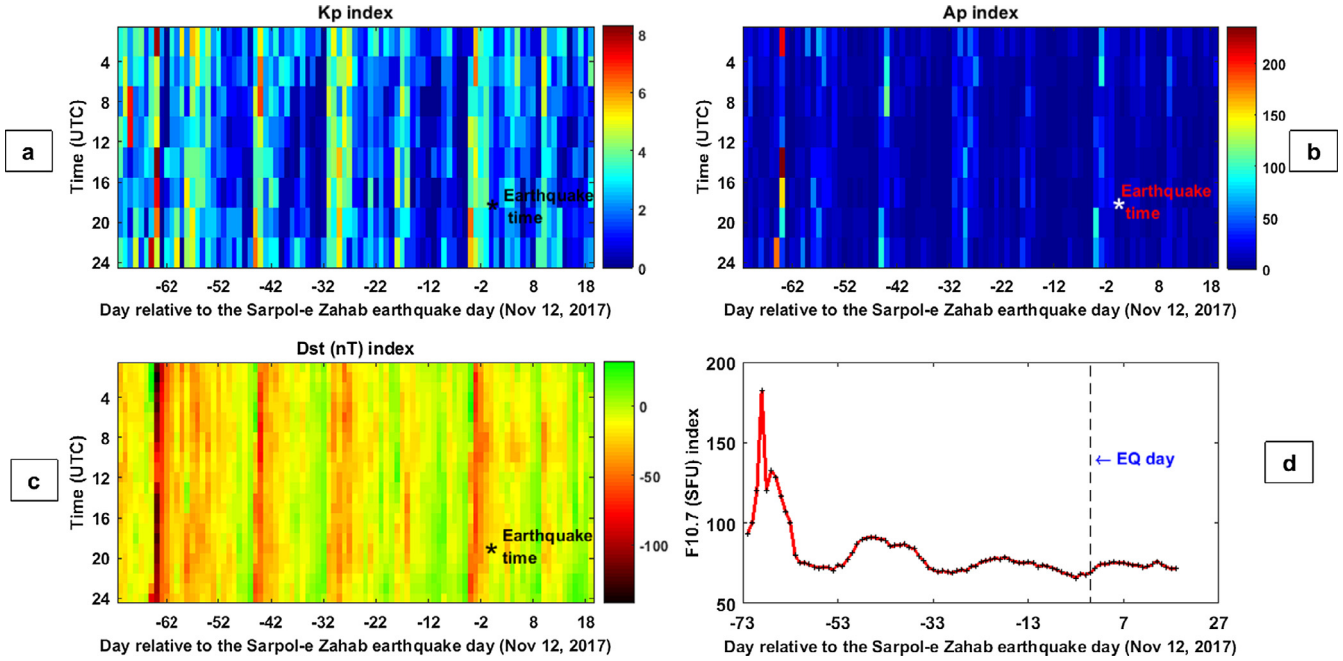

Fig. 2. (a)–(d) show, respectively, the variations of K_p, a_p, D_{st} and solar radio flux (F10.7) indices during the period of 1 September to 30 November 2017. An asterisk in (a)–(c) or a vertical dashed line in (d) indicates the earthquake time. The x-axis represents the days relative to the Iran earthquake day.

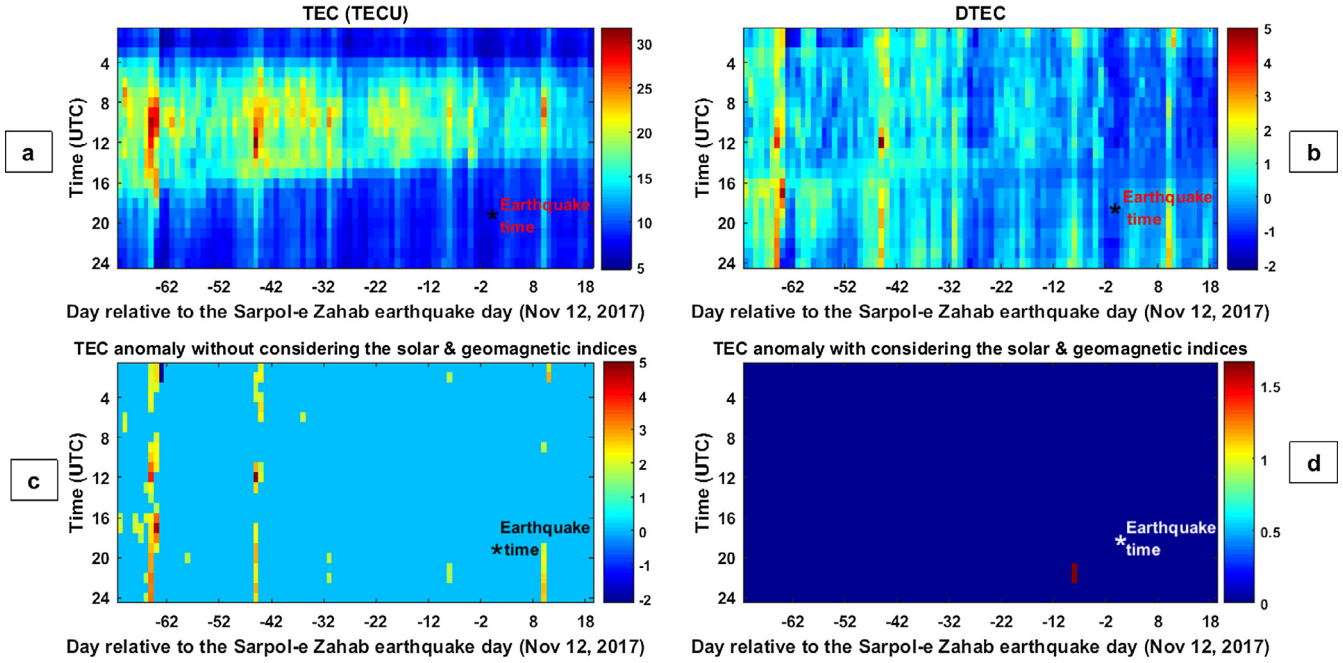

Fig. 3. Results of TEC analysis using Median Method for the Iran earthquake (12 November 2017) from 1st September to 30 November 2017. The earthquake time is indicated by an asterisk. The x-axis represents the day relative to the earthquake day. The y-axis represents the time UTC (LT = UTC-5:00). (a) TEC variations, (b) DTEC variations obtained by equation as $DTEC = \frac{TEC - Median}{Interquartile}$, (c) detected TEC anomalies when $|DTEC| > 1.5$ and (d) detected TEC anomalies when Kp < 2.5, Dst > −20 nT, Dst < 20 nT and F10.7 < 120 and $|DTEC| > 1.5$.

observed unusual TEC variations during this period cannot be associated to the seismic event. Fig. 3(b) shows variations of DTEC ($DTEC = \frac{TEC - Median}{Interquartile}$). Fig. 3(c) shows detected TEC anomalies using the Median method when $|DTEC| > 1.5$ and considering only quiet conditions of solar and geomagnetic activities. To distinguish the likely seismo-ionospheric perturbations from the solar and geomagnetic activities, four conditions including Kp < 2.5, Dst > −20 nT, Dst < 20 nT and F10.7 < 120 are joined to $|DTEC| > 1.5$ constraint, using AND operator (Fig. 3 (d)). Fig. 3(d) indicates a striking TEC anomaly 9 days before the main shock between 21:00 and 22:00 UTC, when

the DTEC has an increase of the order of 127% and 43%, respectively, from the normal state.

In order to implement the Kalman filter method, the half of data has been used for training to obtain the optimum parameters. Fig. 4(a) shows the differences between the predicted TEC values using Kalman filter method and the observed TEC values from 24 days before the earthquake to 20 days after it. Fig. 4(b) shows the DTEC values obtained from $Dx = \frac{x-\mu}{\sigma}$, where μ and σ are the mean value and standard deviation of the differences values between the observed and the predicted values using Kalman filter (x) at each hour, respectively. According to this, if the absolute value of Dx would be greater than k, ($|Dx| > k$), the behavior of the relevant parameter (x) is regarded as anomalous. Fig. 4(c) shows detected TEC anomalies using the median method when $|DTEC| > 1.5$ and in quiet conditions of solar and geomagnetic activities. Fig. 4(d) illustrates the detected TEC anomalies when Kp < 2.5, Dst > -20 nT, Dst < 20 nT and F10.7 < 120 and $|DTEC| > 1.5$. Fig. 4(d) illustrates a striking anomaly 11 days before the earthquake at 16:00 UTC. On this time, the DTEC value passes the higher bound by about 16%.

To implement the Neural Network method, half of data was selected as training data. Using the training data, the network parameters are determined and then, based on the constructed pattern vectors in the feature space, the prediction process is performed. In the case of testing process, if the difference value PE_i between the observed value X_i and the predicted value $\hat{X}_i$, is outside the pre-defined bounds $\mu \pm 1.5 \times \sigma$, ($\mu$ and σ are the mean and the standard deviation of PE_i values), an irregular variation is detected.

Fig. 5(a) is a representation of the differences between the observed and the predicted values during the testing set. Fig. 5(b) shows the DTEC values obtained from $Dx = \frac{x-\mu}{\sigma}$,where μ, σ are the mean and standard deviation of differences values (x) at each hour, respectively. In Fig. 5(c), anomalous TEC values are only depicted at times when $|DTEC| > 1.5$. Then to distinguish pre-earthquake anomalies from the other anomalies related to the geomagnetic activities, the five conditions of Kp < 2.5, Dst > -20 nT, Dst < 20 nT and F10.7 < 120 SFU and $|DTEC| > 1.5$ are jointly used using AND operator to construct the irregular variation map. It is seen that the TEC value exceeds the higher bound 11 days before the earthquake at 16:00 UTC by around 19%.

Fig. 6 illustrates the TEC difference map obtained using the mean of TEC maps of 15 days before earthquake day on 20:00 UTC. A clear clamp of anomaly can be observed close to earthquake epicenter.

2.3. Swarm data analysis

Dobrovolsky et al. (1979) showed, on the basis of a theoretical model, that the radius of the affected area by the precursory effects of an impending earthquake can be estimated using the formula $R = 10^{0.43M}$, where R is the radius in kilometres of the earthquake preparation zone and M is the earthquake magnitude. Therefore, to detect the likely seismo-ionospheric anomalies, we analysed the whole tracks of satellites A, B and C crossing the Dobrovolsky's circular region within R $\approx$ 1000 km from the Iran earthquake epicenter during the period of 1 August to 30 November 2017.

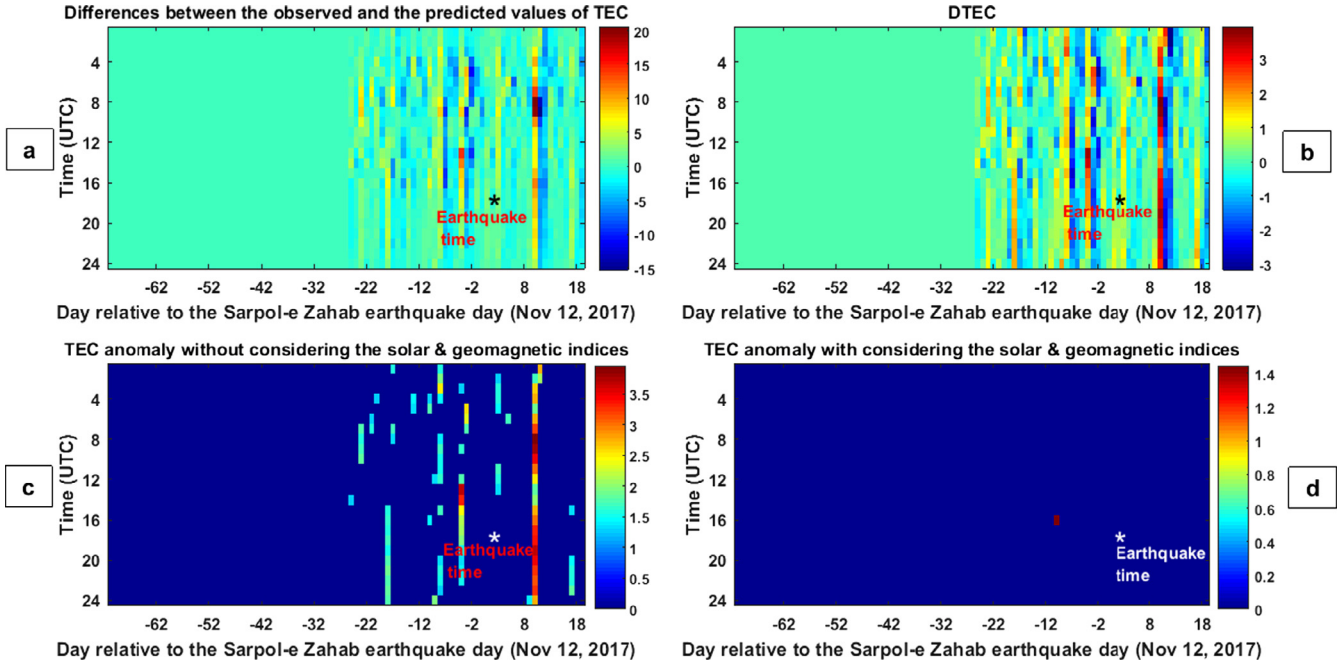

Fig. 4. (a) Differences between the observed and the predicted values of TEC obtained using Kalman filter method. (b) DTEC variations. (c) Detected anomalies using Kalman filter method without considering the non-quiet conditions of solar and geomagnetic activities. (d) Detected TEC anomalies when Kp < 2.5, Dst > -20 nT, Dst < 20 nT and F10.7 < 120 and $|DTEC| > 1.5$.

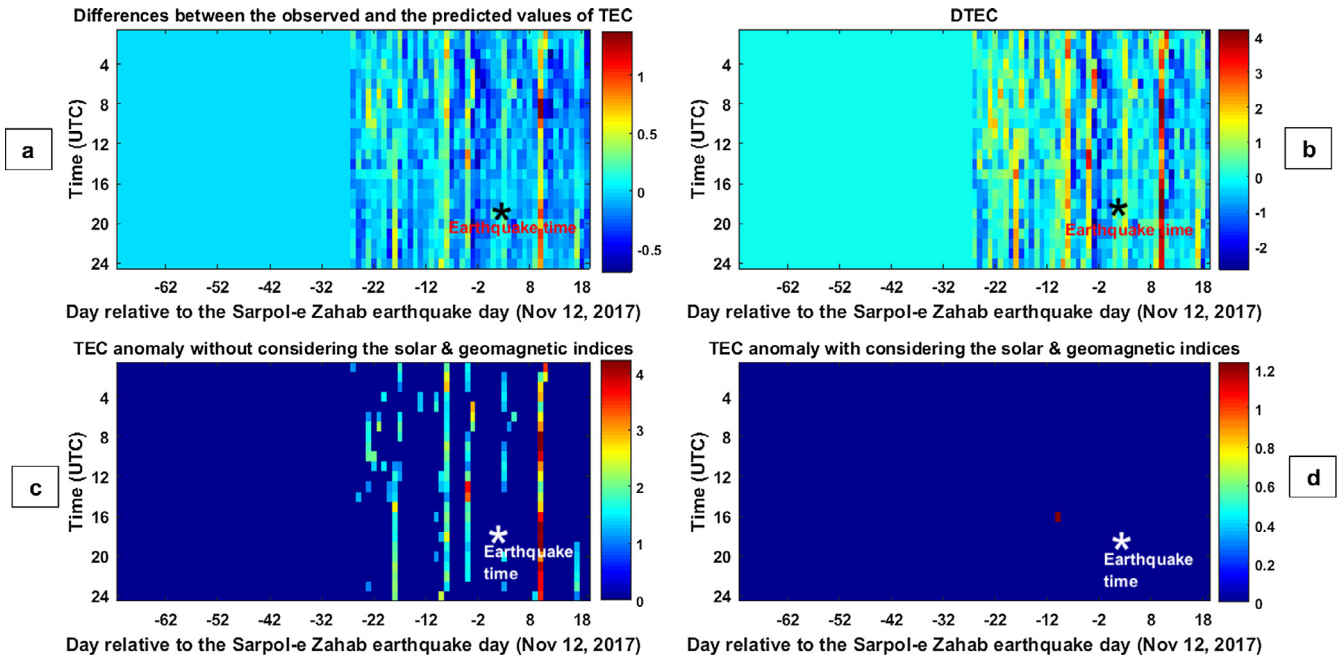

Fig. 5. (a) Differences between the observed and the predicted values of TEC obtained using Neural Network method. (b) DTEC variations. (c) Detected anomalies using Neural Network method without considering the geomagnetic indices. (d) Detected TEC anomalies when Kp < 2.5, Dst > −20 nT, Dst < 20 nT and F10.7 < 120 and $|DTEC| > 1.5$.

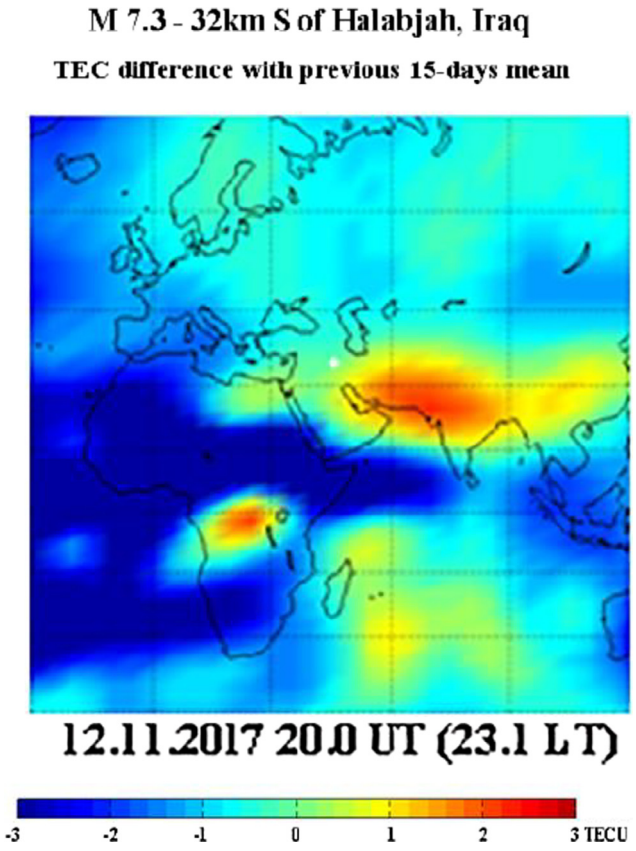

Fig. 6. TEC difference map on the earthquake day.

Fig. 11a shows the track of satellite A crossing the Dobrovolsky's area 9 days before the main shock. The earthquake epicenter, the track and the Dobrovolsky's area are shown as a green star, a red line and a green circle, respectively. The satellite passed southward the Dobrovolsky's area between 02:02:24 and 02:08:46 UTC.

To construct the time series, for each sample the differences ΔN_e and ΔT_e, between the measured electron density and temperature using Swarm satellites, and the corresponding values modelled by IRI2016 (Bilitza et al., 2017) were calculated. Then, for each day, the median of the residuals for each parameter, including the electron density and the electron temperature, separately for day and night tracks, was obtained and, consequently, the time-series of the median values, for day and night during the studied period, were constructed. But since the variations of the plasma parameters affected by nonlinear variations and unfortunately the IRI-model does not fit well all variations of ionosphere, a polynomial of degree 3 fitted to the time series and the residuals between the two curves as a new time series was obtained (Akhoondzadeh et al., 2018; Marchetti and Akhoondzadeh, 2018). Although the use of IRI is not the best, with this combination it provides robustness to our results.

Fig. 7 shows the Swarm A satellite night-time electron density residual variations during the period of 1 August to 30 November 2017. The abscissa represents the days relative to the earthquake day. The vertical dotted line shows the earthquake date. Median, and higher and lower bounds are drawn as blue and green horizontal lines, respectively. The pre-defined allowed ranges are defined as $M \pm 1.25 \times IQR$ which M and IQR are the median and the inter-quartile range parameters, respectively. In the figure, the days accompanied with high geomagnetic activities

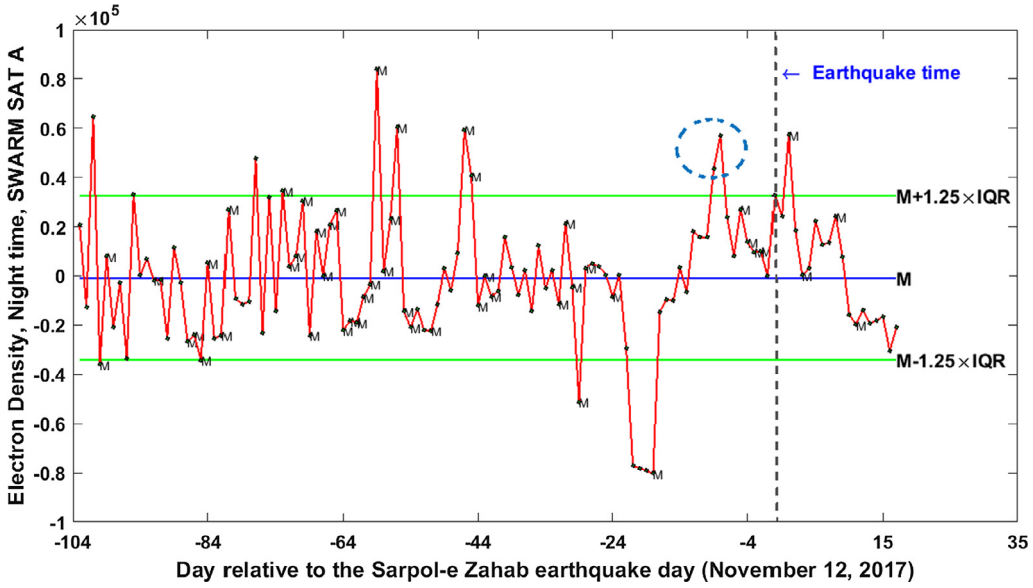

Fig. 7. Results of Swarm A night-time electron density data analysis for the Iran earthquake (12 November 2017) from 01 August to 30 November 2017. The earthquake day is represented as a vertical dashed line. The green horizontal lines indicate the upper and lower bounds ($M \pm 1.25 \times IQR$). The blue horizontal line indicates the median value (M). The values of the median and the allowable bounds were calculated only using the quiet geomagnetic days. The x-axis represents the day relative to the earthquake day. The y-axis represents the Swarm satellite A night-time electron density median values for each day inside the Dobrovolsky's area. Blue circles underline the anomalous positive values. (For interpretation of the references to colour in this figure legend, the reader is referred to the web version of this article.)

are depicted with the M symbol. It should be noted that the values of the median and the allowable bounds were calculated only using the quiet geomagnetic days. This figure shows two positive anomalies on 8 and 9 days before the earthquake day, when the variations of the electron density exceed the higher bound with the values of 74.34% and 33.37% of the higher bound, respectively.

Fortunately, the electron temperature variations acknowledge an observed anomalous variation when it exceeds the lower bound with the value of −18.3% on 9 days before the event (Fig. 8). Also around 40 days before the earthquake there is a positive electron temperature anomaly, but it could be probably due the external perturbation as in the close days the geomagnetic activity is rather high.

Fig. 9 shows the Swarm B satellite electron density residual night-time variations during the period of 01 August to 30 November 2017. It is seen that this parameter indicates an anomaly on 9 days prior to earthquake with the value of 9.8% above the higher bound. Another unusual variation is also observed 35 days before the earthquake.

Fig. 10 illustrates the Swarm C satellite night-time electron density residual variations and an unusual variation on 9 days before the event with the value of 16.3% above the higher bound.

It is interesting that the variations of ΔN_e and ΔT_e parameters measured by all three Swarm satellites of A, B and C, indicate an anomaly on 9 days before the earthquake that it is also at about the same time of TEC anomaly.

In order to perform proper orbital analysis, the night-time tracks of satellites A, B and C on the anomalous date (03 November 2017, i.e. 9 days before the event) were investigated in detail. Figs. 11–13(a) show the mentioned tracks inside the Dobrovolsky's area, on 3 November 2017. The earthquake epicenter, the track and the Dobrovolsky's area are shown as a red asterisk, a red line and a green circle, respectively. The differences between the time-series of the measured electron density/temperature and a fitted polynomial of degree 12 along this track are shown in Figs. 11–13(b) and (c). The vertical axis represents the geomagnetic latitude. An unusual variation in the time series of the residual curve of the electron density is clearly seen close to the earthquake location (the red arrow in Figs. 11–13(b)).

In order to detect the possible magnetic field anomalies in the measurements of both scalar and vector magnetometers, at the first step the difference between the measured parameter in nominal satellite conditions and the predicted value using the IGRF (International Geomagnetic Reference Field) model was calculated. At the next step, the median of the residuals of magnetic values of the tracks was obtained for each day and finally the time-series of the magnetic field median values during the period of 01 August to 30 November 2017 was constructed. To remove the seasonal variations (and all smoothed variations not predicted by the IGRF) a polynomial of degree 3 was fitted to the time series and the residuals values were calculated. If the residual value exceeds the pre-defined threshold value (i.e. $M \pm 1.25 \times IQR$; M and IQR are the median and the inter-quartile range parameters, respectively), the observed

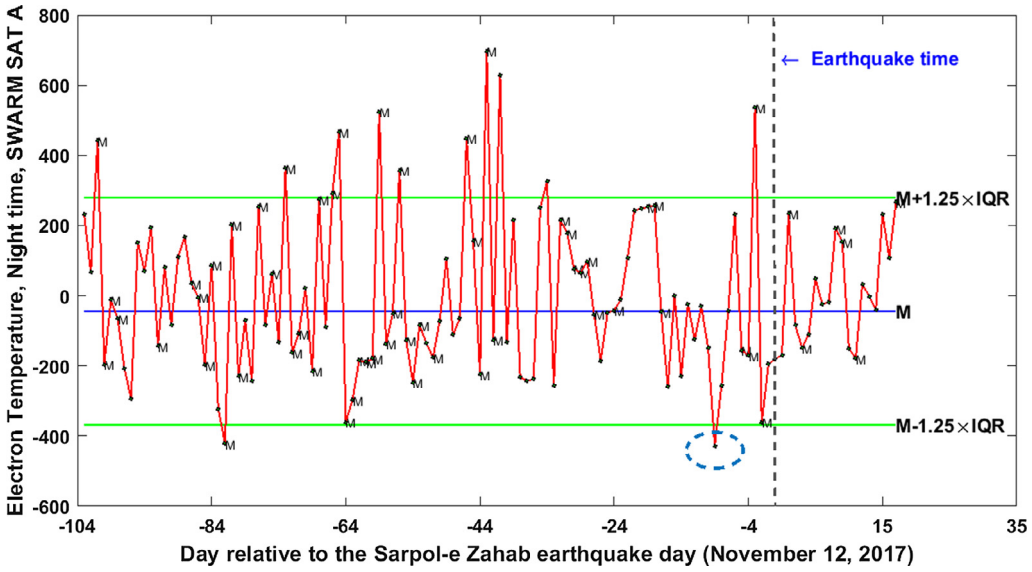

Fig. 8. Same as Fig. 7 but for electron temperature variations.

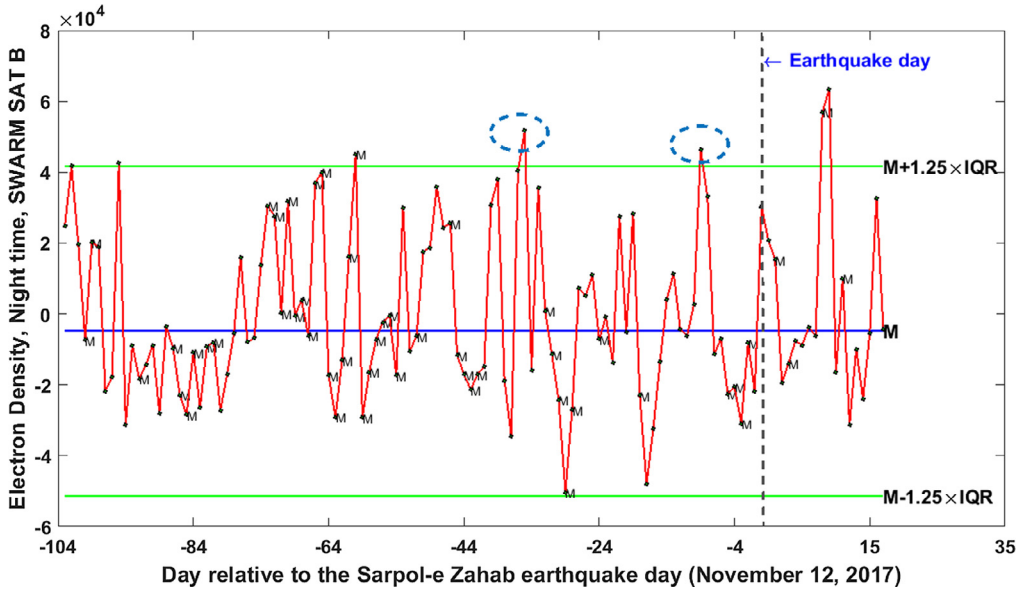

Fig. 9. Same as Fig. 7 but for Swarm B.

parameter in geomagnetically quiet conditions (|Dst| $\leq$ 20 nT, $a_p < 10$ nT)) is regarded as a candidate of a seismic anomaly (Akhoondzadeh et al., 2018; Marchetti and Akhoondzadeh, 2018).

Results of Swarm Alpha, Bravo and Charlie vector Y magnetic field data analysis from 1 August to 30 November 2017 are shown in Fig. 14. Only the magnetically quiet days are represented. The mentioned parameter exceeds the bounds 7 times: 95, 75, 49, 48, 24, 21 and 8 days before the earthquake with the value of 96.1%, 13.6%, 54.8% (negative), 21.3%, 30.9% (negative), 7.5% and 8.4% respectively. The most interesting anomalies are the first for its intensity (roughly 2 times above the median with respect to the threshold) and the 2 consecutive anomalies 49 and 48 days before the earthquake that detect a rapid (in one day) opposite variation of East component of magnetic field with respect to the typical field.

A similar analysis was performed on the absolute scalar intensity of magnetic field and it is shown in Fig. 15. During the investigated time, the magnetic field overpasses the higher bound 4 times: 96, 39, 34 and 11/10 days before the earthquakes with 2.7%, 26.7%, 4.0% and 30.6%/44.7% respectively. The most interesting anomaly is that persisting two consecutive days and that precedes the earthquake by 11–10 days. In these days, the other analysis of TEC and electron density found anomalies so this ionospheric alteration detected from different observables could be a good candidate for pre-seismic effect.

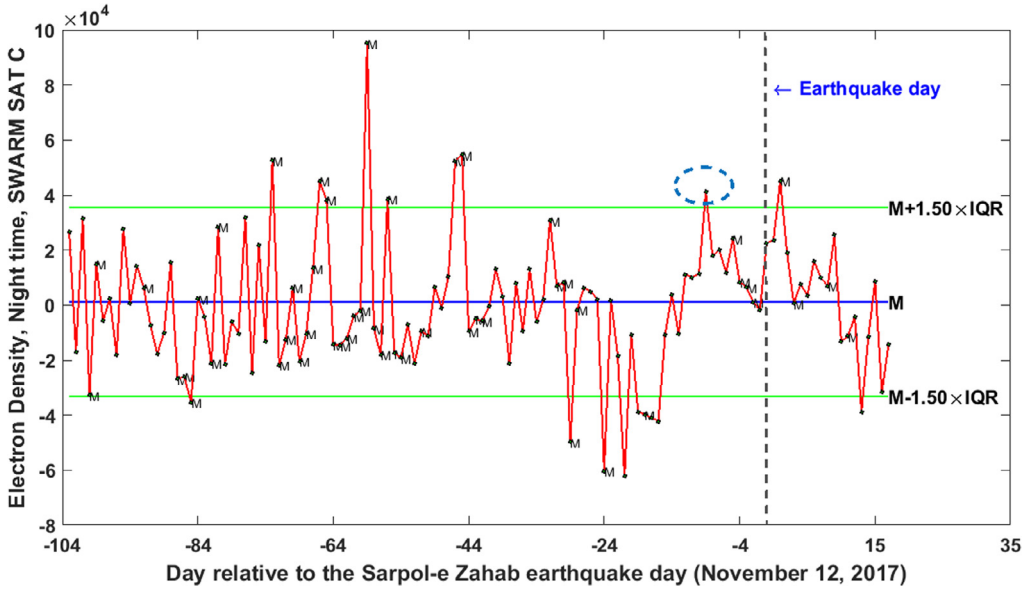

Fig. 10. Same as Fig. 7 but for Swarm C.

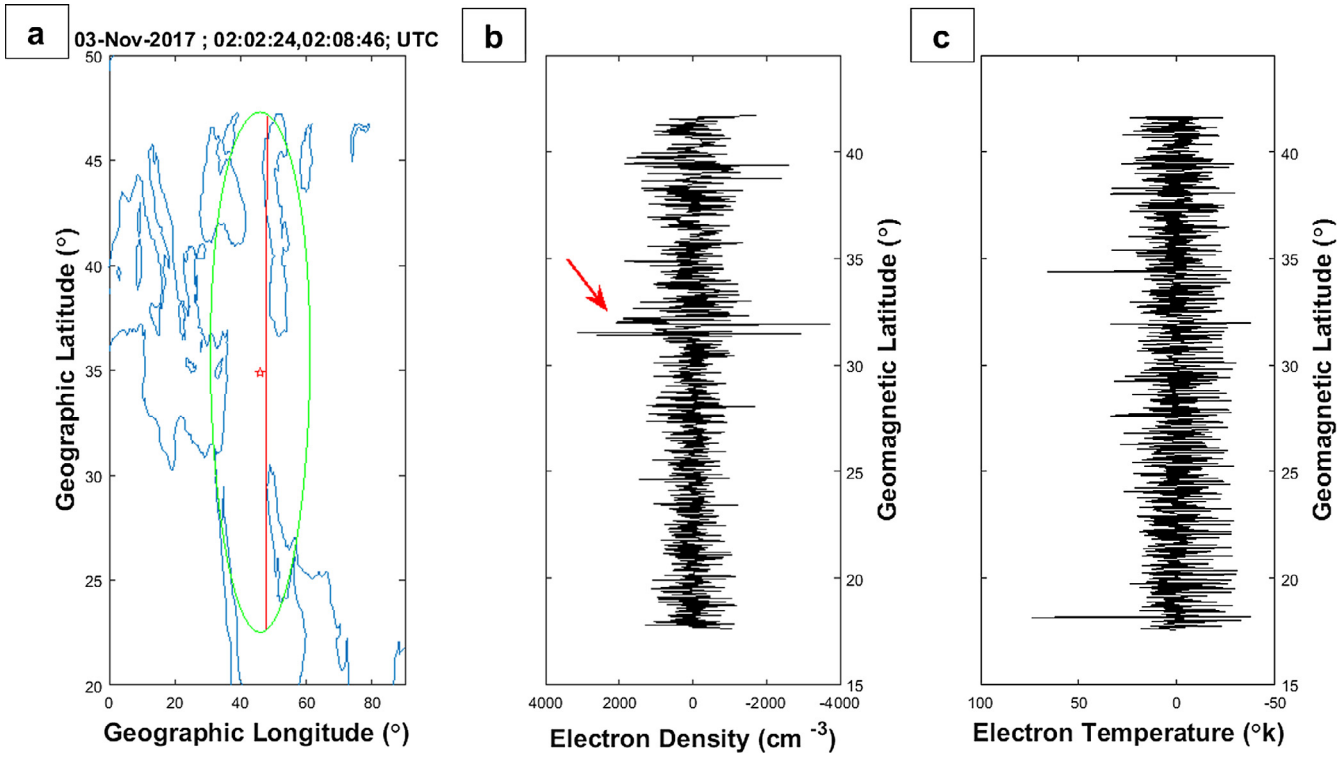

Fig. 11. Results of Swarm A track analysis for the Iran earthquake (12 November 2017) on 3 November 2017, 9 days before the earthquake. (a) The earthquake epicenter, the track and Dobrovolsky's area are shown as a red asterisk, a red line and a green circle, respectively. The track passed the Dobrovolsky's area between the 02:02:24 and 02:08:46 UTC. The horizontal and vertical axes represent the geographic longitude and latitude. (b) and (c) show the differences between the time-series of the measured electron density and temperature and a fitted polynomial of degree 12 along this track. The vertical axis represents the geomagnetic latitude. (For interpretation of the references to colour in this figure legend, the reader is referred to the web version of this article.)

Fig. 16(a) shows the recorded track close to the Iran earthquake epicenter on 03 November, 9 days before the earthquake. The earthquake epicenter, track and Dobrovolsky's area are shown as a green asterisk, a red line and a yellow circle, respectively. The track passed inside the Dobrovolsky's area between the 07:16:18 and 07:24:31 UTC. The horizontal and vertical axes represent the geographic longitude and latitude coordinates, respec-

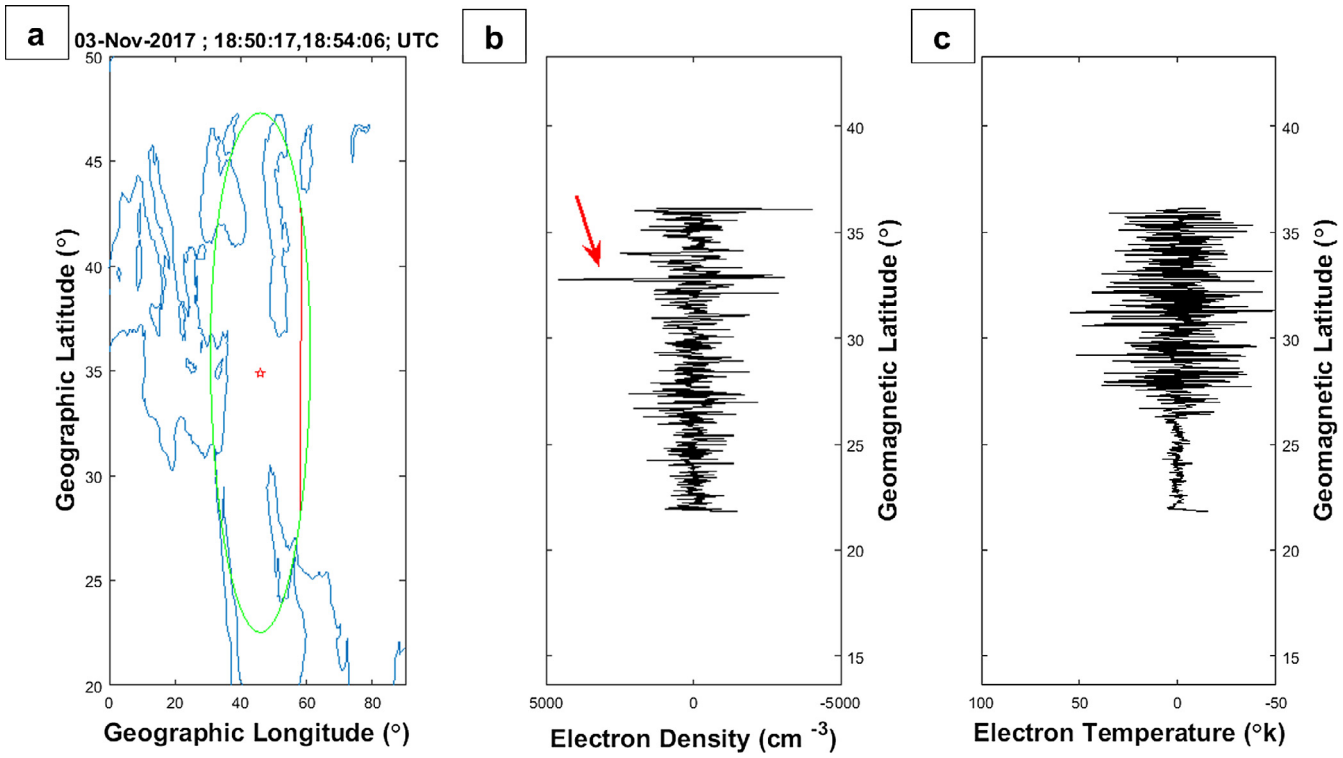

Fig. 12. Same as Fig. 11 but for Swarm B.

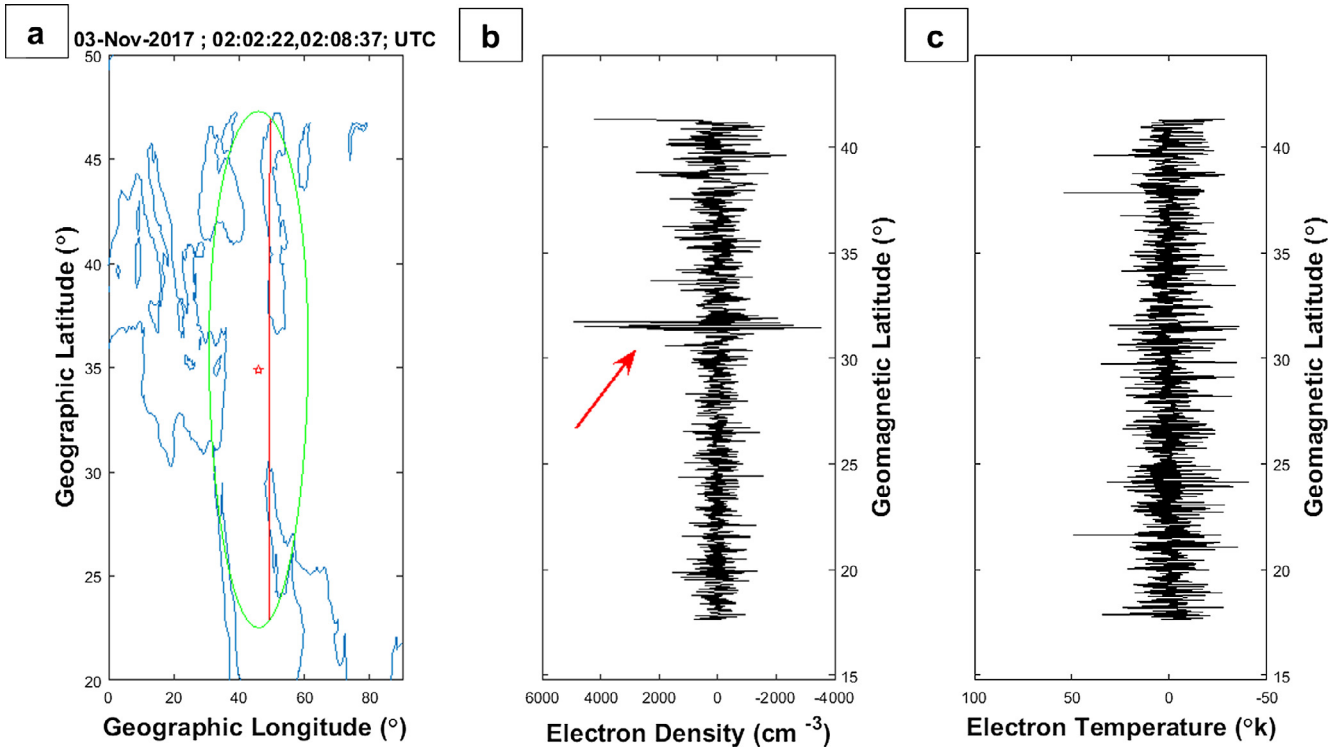

Fig. 13. Same as Fig. 11 but for Swarm C.

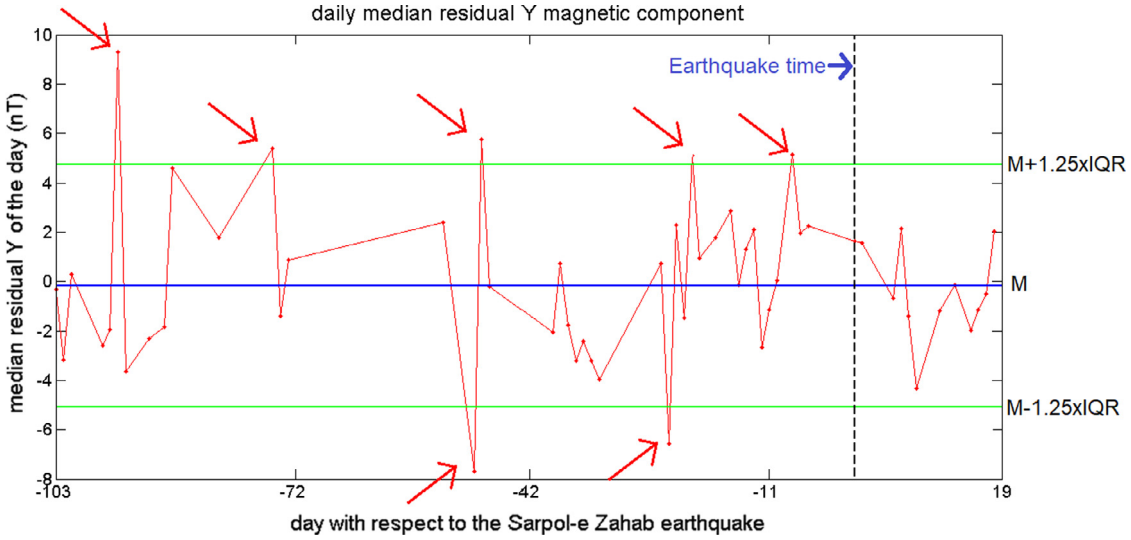

Fig. 14. Results of Swarm Alpha, Bravo and Charlie vector Y magnetic field data analysis for the Iran earthquake (12 November 2017) from 01 August to 30 November 2017.

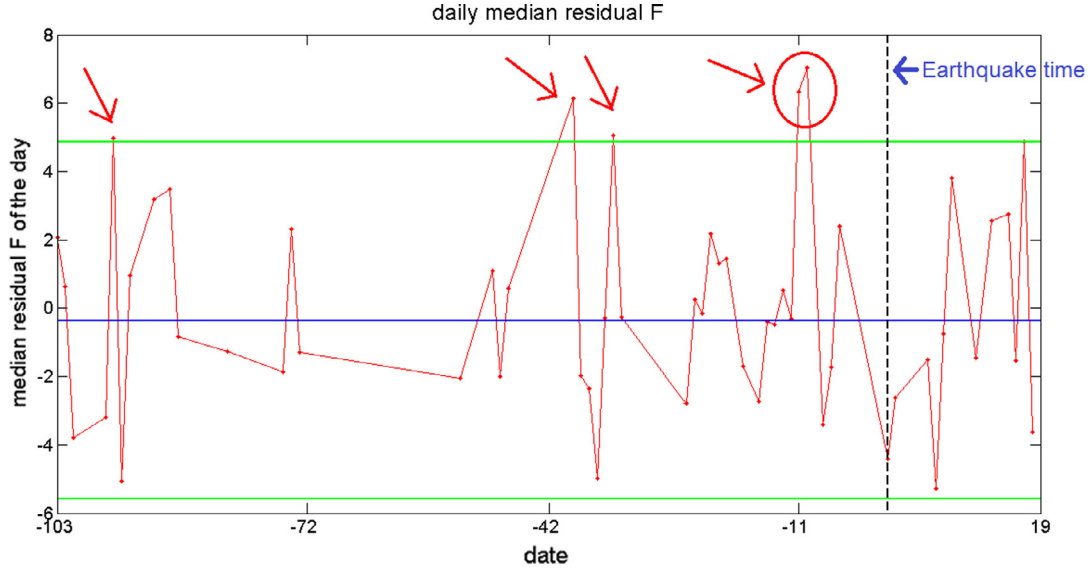

Fig. 15. Results of Swarm Absolute scalar Intensity of magnetic field data analysis for the Iran earthquake (12 November 2017) from 01 August to 30 November 2017.

tively. The residual of the derivatives of the measured magnetic vectors (X, Y, Z) fields and scalar intensity values are shown in Fig. 16. The vertical axis represents the geomagnetic latitude. An unusual variation in the time series of the residual curve of the vector Y of the magnetic field is clearly seen around the earthquake location (the red arrow in Fig. 16).

To check whether some anomalies similar to the one represented in Fig. 16 precede the earthquake occurrence, we apply systematically the MASS (MAgnetic Swarm anomaly detection by Spline analysis) algorithm (already applied successfully to M7.8 Nepal 2015, M7.8 Ecuador 2016 and M8.2 Mexico 2017 earthquakes, published in De Santis et al., 2017, Akhoondzadeh et al., 2018; Marchetti and Akhoondzadeh, 2018, respectively). MASS tags the track inside the Dobrovolsky area as anomalous when it has at least one window with root mean square rms greater than the threshold k_t multiplied for the Root Mean Square RMS computed along the whole track inside +50 and −50 geomagnetic latitude. In this case, we applied a $k_t = 2.5$, so all the tracks with rms > 2.5 RMS are tagged as anomalous. Among all these, only the tracks acquired during geomagnetic quiet conditions are taken into account ($a_p \leq 10$ nT, Dst > −20 nT, Dst < 20 nT). Finally, Fig. 17 shows the cumulative number of the anomalous tracks for the three components of vector magnetic field and its scalar intensity.

Each plot shows three parameters that we used to try to give an objective evaluation of the analysis. R^2 is the square of the Residual correlation coefficient of a linear fit. We

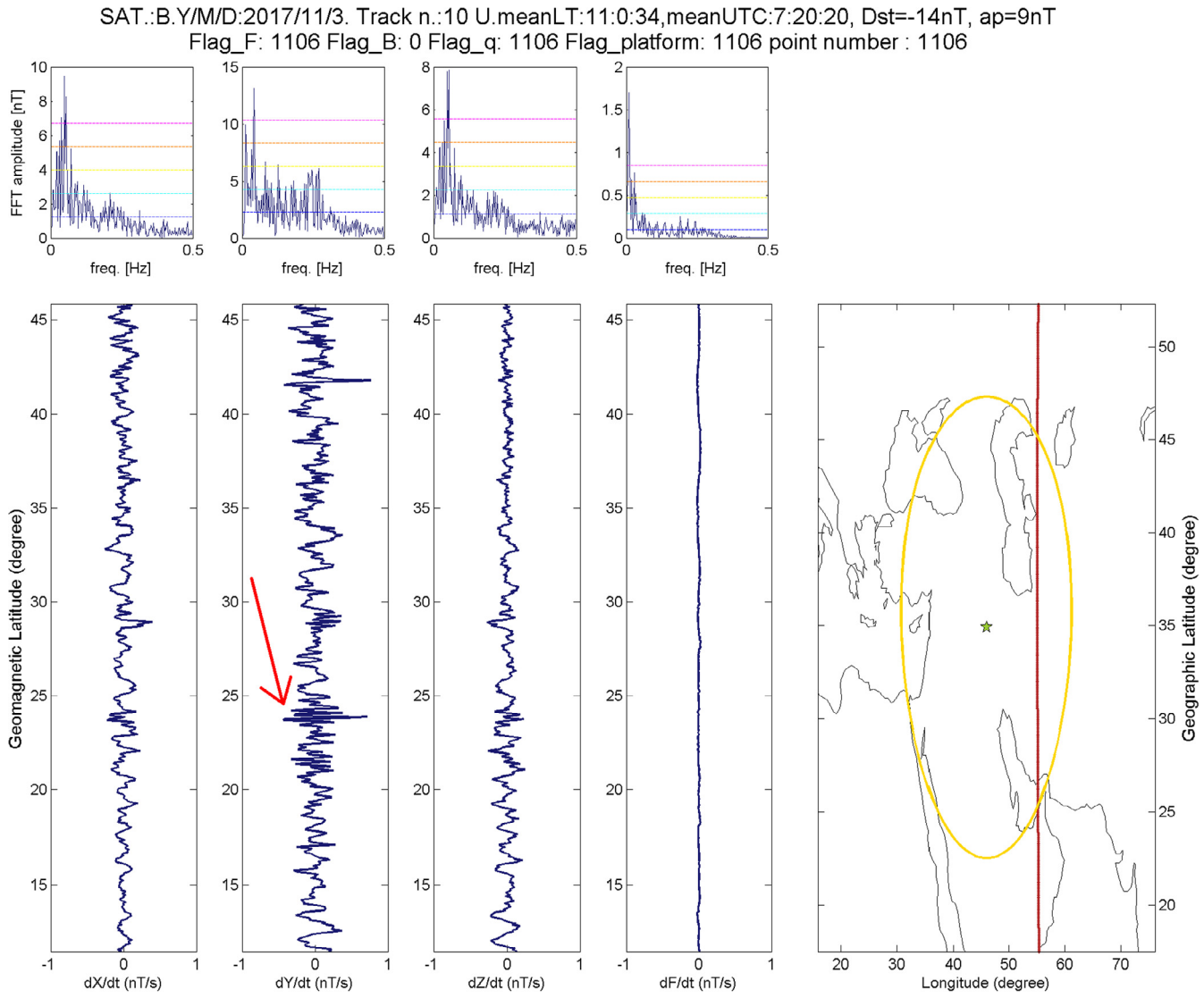

Fig. 16. Results of Swarm B track analysis for the Iran earthquake (12 November 2017) 9 days before the earthquake. The earthquake epicenter, the track and Dobrovolsky's area are shown as a green star, a red line and a yellow circle, respectively in the right map. The track passed the Dobrovolsky's area between the 07:16:18 and 07:24:31 UTC. The horizontal and vertical axes represent the geographic longitude and latitude. The first four plots show the residuals of the derivatives of the measured magnetic vectors (X, Y, Z) fields and scalar intensity values, respectively. The vertical axis represents the geomagnetic latitude. Above the time track, the Fast Fourier Transform analysis of each residual is shown. This analysis is performed inside the minimum and maxim Dobrovolsky latitudes of the region. (For interpretation of the references to colour in this figure legend, the reader is referred to the web version of this article.)

classified as good those analysis that have $R^2 < 0.7$ since we expect that, in case of physical relation of the detected anomalies with the seismic phenomena, the curve must be different from linearity. nEQ is the ratio between the number of the anomalies that follow the earthquake and that one of those that precede the earthquake. As we are searching for precursors, we would like that nEQ is <1. C is the ratio between the number of the anomalies by Bravo satellite and the half sum of the anomalies by Alpha and Charlie. We classified as good the analysis with $C < 1$ as Alpha and Charlie satellites fly at a lower orbit, so we expect a higher probability to detect lithospheric anomalies with respect to Bravo satellite. nEQ^* and C^* are the two parameters normalized by the number of analysed tracks (so also for the selection for geomagnetic quiet time). In this analysis, most of the coefficients pass the test: 9 out of 12. Therefore, we could affirm that the reliability of this analysis is 75%. Observing the overall shape of the cumulative number, it is possible to notice a clear increase of the anomalies that precede the earthquake by about 20–25 days.

Please note that although the use of models such as IRI and/or IGRF, is not the best (because of some known drawbacks of these two models), its combination with other methods (e.g. residual time series analysis after fitting appropriate polynomials) provides robustness to our results.

To perform a multi-parametric analysis and to investigate for possible alteration of the atmosphere as predicted by the LAIC models, we analyzed Skin Temperature (SKT)

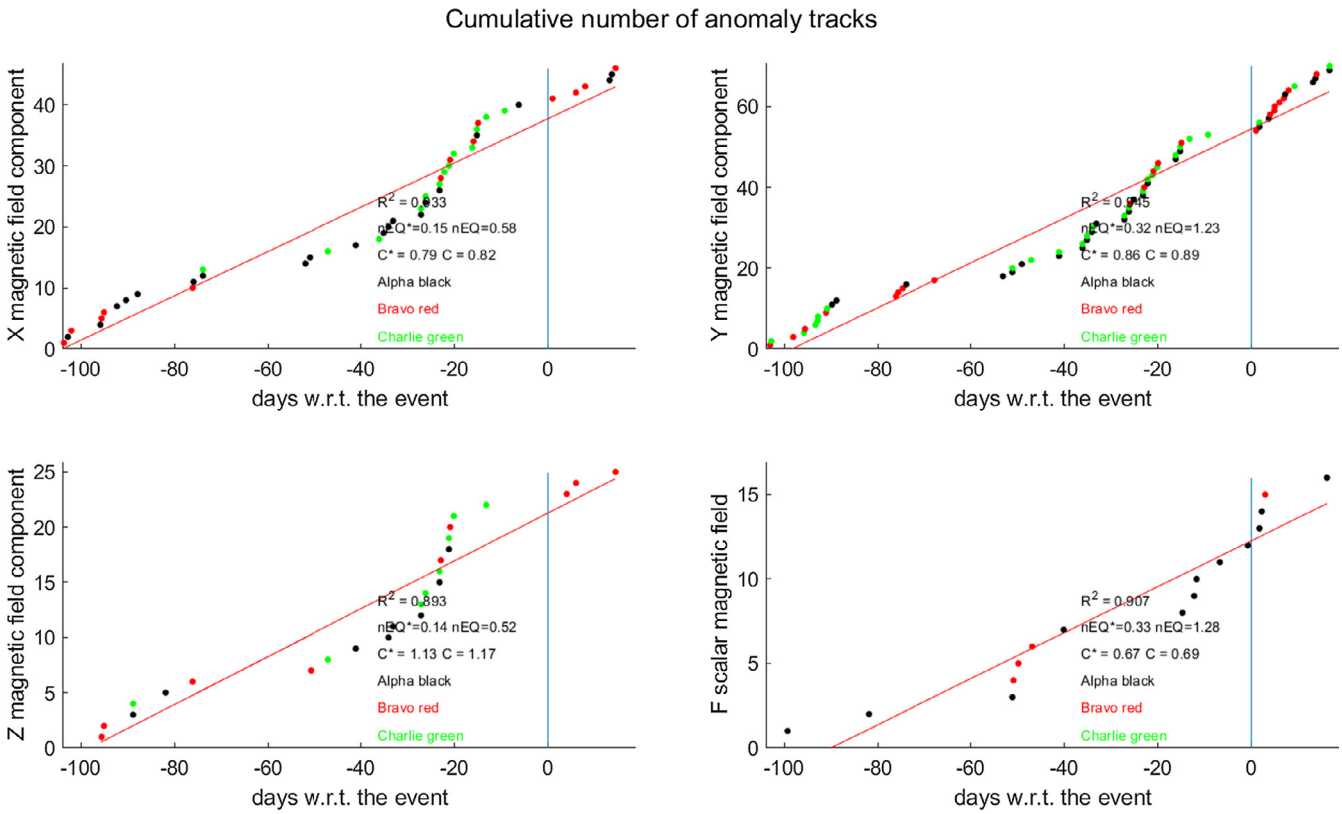

Fig. 17. Cumulative number of anomalies detected by MASS with kt = 2.5 on Swarm Alpha (black dots), Bravo (red dots) and Charlie (green dots), on X, Y and Z components and Absolute scalar Intensity of magnetic field data. The analysis for the Iran earthquake (12 November 2017) starts 1 August and stops on 30 November 2017. The earthquake time occurrence is depicted by vertical blue line. (For interpretation of the references to colour in this figure legend, the reader is referred to the web version of this article.)

and Total Column Water Vapour (TCWV) applying the CAPRI algorithm, as they can be considered reliable seismic precursors (Piscini et al., 2017). In addition, we investigate also other two parameters: Total Aerosol Thickness (AOT) and Sulphur Dioxide (SO_2), retrieved from MERRA-2 dataset. The data analyses are little different overall for the different sources of the data. Basically, we construct a historical time series analyzing each day separately for the mean value and its standard deviation for about 40 years of data. We then compare a reasonable period of the 2017 that includes the earthquake, with the historical mean behavior along the same period (e.g. 4 months): if a value of the 2017 overpasses 2 standard deviations the historical mean behaviour, we define that value as anomalous.

Fig. 18 shows the time series for SKT, TCWV, AOT and SO_2 for about 4 months before the earthquake occurrence in a square region of about 3 degree size around the epicenter. The Skin temperature shows an anomalous day preceding the earthquake by 15 days. For this day, in Fig. 18 is included the map of the distribution of the skin temperature differences with respect to historical mean values and minus a typical day (i.e. a day with value close to the historical mean). What it is very interesting is the concentration of the anomaly spatially very close to the epicenter and with some peak values of more than 10 K above the typical value for that region and that time. The Total column water vapour presents an anomalous day (6 days before the earthquake occurrence), followed by two other days with values still above 1.5 standard deviations.

The SKT anomaly that we found is compatible with the one reported by Wu et al. (2018) that preceded the earthquake by two weeks.

AOT graph presents three groups of anomalies that precede the earthquake by 87 days (single very high anomaly: 3.8σ), 53–47 days (two couples of consecutive days), 17–9 days (single + couple of anomalies). SO_2 graph presents three groups of anomalies too, but the first anomaly is time shifted with respect to the first one of the AOT. They precede by 76 days, 54–47–43 days (three single time-close anomalies) and a numerous group of anomalies that precede the seismic event from 19 to 9 days (2 single anomalies + 2 couples of anomalies).

Practically all the investigated atmospheric parameters present some anomalies in the last days of time series that precede the earthquake occurrence from 19 to 6 days. It is very interesting to note that analysis from different dataset (and sources), for example skin temperature from ECMWF and SO2 from MERRA2, present an anomaly on the same day (15 days before the earthquake) giving more reliability to the datasets and to the real perturbation of the atmosphere for that day.

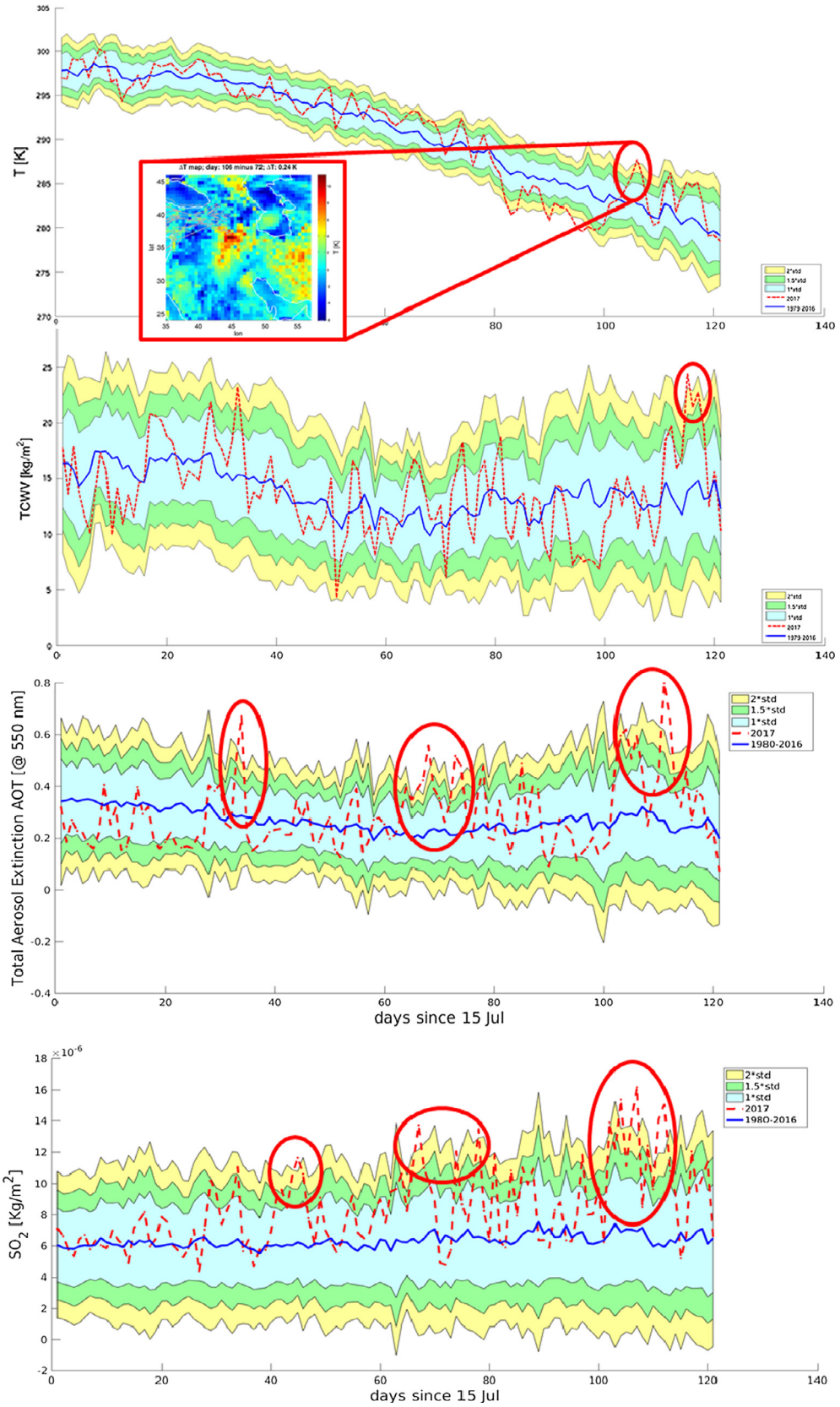

Fig. 18. Meteorological – climatological analysis performed for 120 days preceding the Iran earthquake (12 November 2017) from 15 July to 12 November 2017 (the last day of each time series is the day of the earthquake) for SKT, TCWV, AOT and SO_2. Blue line represents the historical mean, light blue, green and yellow bars show 1.0, 1.5 and 2.0 standard deviations, respectively, and the red dashed line represents the value in the earthquake year (2017). (For interpretation of the references to colour in this figure legend, the reader is referred to the web version of this article.)

Table 1
The list of the detected anomalies. Day is relative to the earthquake day.

Parameter	Day	Time (LT)
TEC (Median method)	−9	21:00
		22:00
TEC (Kalman filter method)	−11	16:00
TEC (ANN method)	−11	16:00
Electron density, Swarm A satellite	−101	Night
	−77	Night
	−8	Night
	−9	Night
Electron temperature, Swarm A satellite	−9	Night
Electron density, Swarm B satellite	−35	Night
	−9	Night
Electron density, Swarm C satellite	−9	Night
Magnetic field, Vector Y, Swarm satellites	−95	
	−75	
	−49	
	−48	
	−24	
	−21	
	−8	
F Magnetic field intensity, Swarm satellites	−96	
	−39	
	−34	
	−11	
	−10	
Swarm multi components MASS analysis	−25:−20	
SKT (2 standard deviations)	−15	Night
TCWV (2 standard deviations)	−85:−90	Night
AOT (2 standard deviations)	−87	Night
	−53:−47	
	−17:−9	
SO_2 (2 standard deviations)	−76	Night
	−54:−43	
	−19:−9	

The characteristics of the detected anomalies in the variations of discussed parameters are listed in Table 1.

3. Conclusions

In this study, three standard, classical and intelligent methods including Median, Kalman filter and Neural Network were applied to detect the anomalous variations in the time series of the three months of GPS TEC measurements around the time and location of the Iran earthquake (November 12, 2017). The mentioned methods showed striking anomalies 9 and 11 days prior to this earthquake. It is seen that Kalman filter and ANN methods detected anomaly 11 days prior to the studied event which is slightly different from the date of observed anomaly by median method, i.e. on 9 days before the earthquake. It should be noted that the sensitivity of Kalman filter and ANN method to complexity and non-linearity behaviors of TEC time series is more than the median method. It is interesting that these two suggested methods for anomaly detection in TEC time series present the same results and can be implemented instead of the simple methods such as the median.

Furthermore, a comparative study using the six measured parameters from Swarm satellites (Alpha, Bravo and Charlie) has been done and clear anomalies were seen between 8 and 11 days before the event. The quiet solar-geomagnetic conditions during the period of the observed ionospheric anomalies permits us to affirm that they are not related to the solar activity or other external disturbance and this is a good base to search for seismic source anomalies. Moreover, in the same time, according to Liu (2018) a ionospheric disturbance was independently detected by FORMOSAT-5 in ion density and TEC 7–9 days before the earthquake occurrence.

To better understand the preparatory phase of the Iran 12 November 2017 earthquake we investigated also four atmospheric meteorological/climatological parameters to detect possible chemical/physical alteration of the atmosphere: skin temperature, total column water vapour, aerosol optical thickness and sulphur dioxide. All investigated parameters present some anomalies distributed in different times, but most of all seem to indicate a final disturbance of the atmosphere that precedes by some days the ionospheric disturbance in TEC, Ne and magnetic data. This is a very interesting feature, as a lithospheric activity is expected to disturb before the atmosphere and then the ionosphere as it propagates upwards.

So far, different hypotheses about the behavior of earthquake precursors have been discussed based on geophysical and geochemical processes. However, it is still challenging to understand precursor mechanism. The Multi precursor's analysis that we applied in this work seems to be the best way to approach the problem so far. The sequence of different anomalies would confirm a bottom-up LAIC process. Our results show that the anomaly excited by earthquake probably does exist but its use for operational prediction is still questionable, if not hardly possible. On the other hand, what we are doing further on, i.e. use of simultaneous anomalies in different parameters, is probably the only way of possible predictions. We think this work is a further step toward a better exploitation of the complex problem of lithosphere-atmosphere-ionosphere coupling, including for instance the identification of other alternative effects due to other phenomena such as meteorological, climatological or volcanic processes (e.g. Piscini et al., 2019).

Acknowledgement

The authors would like to acknowledge the ESA for the Swarm data, NASA Jet Propulsion Laboratory for the TEC data (ftp://cddis.gsfc.nasa.gov/), solar and geomagnetic indices (ftp://ftp.ngdc.noaa.gov/). This work was supported financially by Iran National Science Foundation (INSF) and founded with project No. 53729. This work was undertaken also in the framework of the ESA-funded project SAFE (Swarm for Earthquake study) and ASI founded project LIMADOU-Science. Two anonymous referees are thanked for their suggestions and comments that improved the work significantly.

References

Akhoondzadeh, M., 2012. Anomalous TEC variations associated with the powerful Tohoku earthquake of 11 March 2011. Nat. Hazards Earth Syst. Sci. 12, 1453–1462.

Akhoondzadeh, M., 2013. A MLP neural network as an investigator of TEC time series to detect seismo-ionospheric anomalies. Adv. Space Res. 51, 2048–2057.

Akhoondzadeh, M., De Santis, A., Marchetti, D., Piscini, A., Cianchini, G., 2018. Multi precursors analysis associated with the powerful Ecuador (M_W=7.8) earthquake of 16 April 2016 using Swarm satellites data in conjunction with other multi-platform satellite and ground data. Adv. Space Res. 61, 248–263.

Bilitza, D., Altadill, D., Truhlik, V., Shubin, V., Galkin, I., Reinisch, B., Huang, X., 2017. International reference ionosphere 2016: from ionospheric climate to real-time weather predictions. Space Weather, 1002/2016SW001593.

Dee, D.P., Uppala, S.M., Simmons, A.J., Berrisford, P., Poli, P., Kobayashi, S., Andrae, U., Balmaseda, M.A., Balsamo, G., Bauer, P., Bechtold, P., Beljaars, A.C.M., van de Berg, L., Bidlot, J., Bormann, N., Delsol, C., Dragani, R., Fuentes, M., Geer, A.J., Haimberger, L., Healy, S.B., Hersbach, H., Hólm, E.V., Isaksen, L., Kållberg, P., Köhler, M., Matricardi, M., McNally, A.P., Monge-Sanz, B.M., Morcrette, J.-J., Park, B.-K., Peubey, C., de Rosnay, P., Tavolato, C., Thépaut, J.-N., Vitart, F., 2011. The ERA-Interim reanalysis: configuration and performance of the data assimilation system. Q.J.R. Meteorol. Soc. 137, 553–597. https://doi.org/10.1002/qj.828.

De Santis, A., Balasis, G., Pavón-Carrasco, F.J., Cianchini, G., Mandea, M., 2017. Potential earthquake precursory pattern from space: the 2015 Nepal event as seen by magnetic Swarm satellites. Earth Planet. Sci. Lett. 461, 119–126.

Dobrovolsky, I.R., Zubkov, S.I., Myachkin, V.I., 1979. Estimation of the size of earthquake preparation zones. Pure Appl. Geophys. 117, 1025–1044.

Freund, F., 2009. Stress-activated positive hole charge carriers in rocks and the generation of pre-earthquake signals. In: Hayakawa, M. (Ed.), Electromagnetic Phenomena Associated with Earthquakes. Transworld Research Network, Trivandrum, pp. 41–96.

Gelaro, R., McCarty, W., Suárez, M.J., Todling, R., Molod, A., Takacs, L, Randles, C.A., Darmenov, A., Bosilovich, M.G., Reichle, R., Wargan, K., Coy, L., Cullather, R., Draper, C., Akella, S., Buchard, V., Conaty, A., da Silva, A.M., Gu, W., Kim, G.-K., Koster, R., Lucchesi, R., Merkova, D., Nielsen, J.E., Partyka, G., Pawson, S., Putman, W., Rienecker, M., Schubert, S.D.C, Sienkiewicz, M., Zhao, B., 2017. The Modern-Era Retrospective Analysis for Research and Applications, Version 2 (MERRA-2), American Meteorological Society – Modern-Era Retrospective analysis for Research and Applications version 2 (MERRA-2) special collection.

Haagmans, R., Bock, R., Rider, H., 2013. Swarm; ESA's magnetic field mission. www.ESA.int.

Hayakawa, M., Molchanov, O.A., 2002. Seismo-Electromagnetics: Lithosphere-Atmosphere-Ionosphere Coupling. Terra Scientific Publishing Co., Tokyo, p. 477.

Jin, S.G., Occhipinti, G., Jin, R., 2015. GNSS ionospheric seismology: recent observation evidences and characteristics. Earth-Sci. Rev. 147, 54–64. https://doi.org/10.1016/j.earscirev.2015.05.003.

Liu, J.Y., Chuo, Y.J., Shan, S.J., Tsai, Y.B., Pulinets, S.A., Yu, S.B., 2004. Pre-earthquake-ionospheric anomalies registered by continuous GPS TEC. Ann. Geophys. 22, 1585–1593.

Liu, J.Y., 2018. Seismo-ionospheric precursors of the 2017 M7.3 Iran-Iraq Border Earthquake and the 2018 M5.9 Osaka Earthquake observed by FORMOSAT-5/AIP. EMSEV 2018, International Workshop Integrating Geophysical Observations from Ground to Space for Earthquake and Volcano Investigations Potenza, Italy, September 17–21.

Marchetti, D., Akhoondzadeh, M., 2018. Analysis of Swarm satellites data showing seismo-ionospheric anomalies around the time of the strong Mexico (Mw=8.2) earthquake of 08 September 2017. Adv. Space Res. 62 (3), 614–623.

Parrot, M., 1995. Use of satellites to detect seismo-electromagnetic effects, Main phenomenological features of ionospheric precursors of strong earthquakes. Adv. Space Res. 15 (11), 1337–1347.

Piscini, A., De Santis, A., Marchetti, D., Cianchini, G., 2017. A multi-parametric climatological approach to study the 2016 Amatrice-Norcia (Central Italy) earthquake preparatory phase. Pure appl. Geophys. 174 (10), 3673–3688.

Piscini, A., Marchetti, D., De Santis, A., 2019. Multi-Parametric Climatological Analysis Associated with Global Significant Volcanic Eruptions During 2002–2017. Geophys. Pure Appl., in press

Pulinets, S.A., Boyarchuk, K.A., 2004. Ionospheric Precursors of Earthquakes. Springer, Berlin.

Pulinets, S., Ouzounov, D., 2011. Lithosphere-Atmosphere-Ionosphere Coupling (LAIC) model – an unified concept for earthquake precursors validation. J. Asian Earth Sci. 41, 371–382.

Sorokin, V.M., Pokhotelov, O.A., 2014. Model for the VLF/LF radio signal anomalies formation associated with earthquakes. Adv. Space Res. 54 (12), 2532–2539.

Wu, L., Zhou, Y., Miao, Z., Qin, K., 2018. Anomaly Identification and Validation for Winter 2017 Iraq and Iran Earthquakes. EGU General Assembly, EGU2018-5800.